**NICST_MEMO_08_024**

**NICST Internal Memo**

Date: July 1, 2008
From: J McIntire, C. Pan, and S. Xiong
To: Bruce Guenther, Jim Butler, Jack Xiong
Subject: Updated Analysis Results for VIIRS EDU RC-05 Part 1, Nominal Plateau at 28V

---

References:


[1] NICST_REPORT_06_009, 'Preliminary test analysis report of VIIRS EDU RC-05 Parts 1 & 2 in TV at Nominal Plateau,' August 4, 2006.
[2] NICST_REPORT_06_025, 'Radiometric Characterization Report of EDU RC-05 Part1 Using BCS at Hot Plateau (28V) and Comparison with Cold & Nominal,' December 13, 2006.
[3] 'Performance Specification Sensor Specification,' ps154640-101c.
[4] Y21901, 'VIIRS Test Analysis report for RC-05, Part 1 Bands M12-M16, I4-I5,' Mina Mitani and Heidi Warner, January 17, 2007.
[5] Y22061, 'VIIRS Test Analysis Report for RC-05, Part 1,' Courtney Ranshaw and Mina Mitani, January 26, 2007.
[6] '2nd Order Radiometric Calibration pf Emissive Bands (RC-5 Part 1),' Courtney Ranshaw, December 13, 2006.
[7] Y18352, 'Performance Verification Review: Thermal Emissive Band Radiometric response Characterization (RC-3 and RC-5 Tests),' Eric Johnson and Jim Young, January 18, 2006.
[8] 'Sensor Performance Verification Plan,' PVP154640-101.
[9] 'EFR2836 Status –MWIR Only,' Mark Bliton and Brendan Robinson, January 28, 2008.


## 1. Introduction

This memo presents an update to the analysis results [1-2] from the VIIRS EDU RC-05 Part 1 test for the Nominal Plateau at 28V. RC-05 was conducted during the Thermal Vacuum (TVAC) portion of the calibration testing, in which the VIIRS instrument was held at near space-like conditions. The purpose of the RC-05 test was radiometric characterization of the Thermal Emissive Bands (TEB). This test was divided into two parts: the first part assesses the response to the Blackbody Calibration Source (BCS) and Three Mirror Collimator (TMC) blackbody. This memo will present the radiometric gains and will consider the sensor performance against a number of specifications [3]. The results of this analysis are compared to Raytheon [4-6].

Table 1 lists the relevant UAIDs along with their corresponding BCS and TMC temperatures. The BCS and TMC data is contained in separate collects. Each collect contains 100 scans. The BCS source was located in the last collect window and the TMC source was located in the middle collect window. In addition, the Space View Source (SVS) was positioned in the Space View (SV) port. The TMC source was used to access the low gain region of band M13. The VIIRS sensor was operated in diagnostic mode. The general outline of the methodology used in this work follows from [7-8] with some modifications.

## 2. Data processing

The VIIRS EDU TV tests were conducted using the F9 aperture. However, all of the specifications for the VIIRS sensor assume a F6 aperture. In order to convert the specifications for comparison to the F9 data, the following factor was employed:

$$L_{F9} = L_{F6}\left(\frac{9}{6}\right)^2 . \quad (1)$$

Notice that it is the radiances that are scaled. In the cases were a temperature needs to be converted, the temperature is first translated into a radiance using the Planck radiation law, then the correction factor is employed, and finally the inverse of the Planck radiation law is used to acquire the appropriate F9 temperature.

The data analyzed here is restricted to a subset of the available samples in a given collect for which the source (either BCS or TMC) yielded a stable response. The following sample ranges were used in this work: samples 1650 – 1849 for a M band using the BCS; samples 3300 – 3699 for an I band using the BCS; and samples 1340 – 1439 for M13 using the TMC. Note that the BCS and TMC data is in separate collects.

The response was analyzed using the scan method. First, the $DN_{SV}$ was averaged over all samples in a given scan. Then, $<DN_{SV}>_{samples}$ was subtracted from each sample of the $DN_{EV}$. Next, the dn was averaged first over samples and then over scans, or $<<dn>_{samples}>_{scans}$. The standard deviation of all samples in a given scan was calculated; the average of these standard deviations for all scans was then performed, or $<\sigma>_{scans}$. Note that the HAM sides alternate from scan to scan such that there are 50 scans for each HAM side. Additionally, the I band data is divided into two subsamples where the larger is always labeled subsample 1. This process is conducted separately for both the BCS and TMC sources.

The temperatures ($T_{xxx}$) of the following were extracted: BCS, TMC, SVS, HAM, and Rotating Telescope Assembly (RTA). The HAM and RTA temperatures were acquired using the LRV extractor and the BCS and SVS temperatures were obtained from the gse files. Note that, due to lack of availability, the TMC temperature was acquired from the adf files.

For each of these temperatures, a Planck radiation was calculated using the center wavelength ($\lambda$) of each band and the equation

$$L_{xxx}(\lambda, T_{xxx}) = \frac{2hc}{\lambda^5}\frac{1}{e^{hc/\lambda k T_{xxx}} - 1}. \quad (2)$$

Then, the Relative Spectral Response (RSR) was applied as a correction to the Planck radiances; this was implemented by the following equation

$$\langle L_{xxx}(B,D,H,T_{xxx})\rangle = \frac{\int RSR(B,D,\lambda)\, L_{xxx}(B,H,T_{xxx})\, d\lambda}{\int RSR(B,D,\lambda)\, d\lambda}, \quad (3)$$

where B, D, and H represent band, detector, and HAM side, respectively. The RSR data was available for only some detectors; therefore, the existing RSR was extrapolated to the missing detectors.

## 2.1 Low Temperature

Now we separate the analysis into two regions, low and high temperature. For the low temperature portion, both BCS and TMC sources are considered (UAIDs 2002504 – 23 and UAIDs 2002515 – 23, respectively). We begin by calculating the background subtracted source radiance, or

$$\begin{aligned}\Delta L_{xxx}(B,D,H,C) &= rvs(B,\phi_{xxx},H)\langle L_{xxx}(B,D,C)\rangle - rvs(B,\phi_{SVS},H)\langle L_{SVS}(B,D,C)\rangle \\ &+ \frac{rvs(B,\phi_{SVS},H) - rvs(B,\phi_{xxx},H)}{\rho_{RTA}(B)} \\ &\times \langle L_{HAM}(B,D,H,C)\rangle - (1-\rho_{RTA}(B))\langle L_{RTA}(B,D,H,C)\rangle\end{aligned}. \quad (4)$$

This includes contributions to the background from not only the SVS, but from the RTA and HAM as well. In addition, the radiances are corrected for Response Versus Scan angle (RVS) and the reflectance factor ($\rho$) is included. Note that C refers to the collect number (each corresponding to a particular $T_{xxx}$) and that $\varphi_{xxx}$ refers to the HAM angle of incidence for a given source (BCS, TMC, or SVS).

In order to determine the radiometric gains, polynomial fits were conducted to the response versus the delta radiance. Least-squares fits were performed over the dynamic range (F9) at the linear, quadratic, and cubic levels. These polynomials take the from

$$\Delta L_{xxx} = \sum_{i=0}^{N} a_i dn_{xxx}^i. \quad (5)$$

The inverse of the linear term ($1/a_1$) is the radiometric gain. In addition, the fractional fitting residual is defined as

$$\Delta_{fit} = \frac{\Delta L_{xxx} - \sum_{i=0}^{N} a_i dn_{xxx}^i}{\Delta L_{xxx}}. \quad (6)$$

Outlying points were discarded (the only outlier in this analysis was the first point in the dynamic range for band I4). Next, we need to calculate the retrieved calibration source radiance, or

$$\left\langle L_{xxx}\left(B,D,H,C\right)\right\rangle_{retrieved}=\frac{\sum_{i=0}^{N}a_i dn_{xxx}^{i}}{rvs\left(B,\phi_{xxx},H\right)}+\frac{rvs\left(B,\phi_{SVS},H\right)}{rvs\left(B,\phi_{xxx},H\right)}\left\langle L_{SVS}\left(B,D,H,C\right)\right\rangle$$
$$+\frac{rvs\left(B,\phi_{xxx},H\right)-rvs\left(B,\phi_{SVS},H\right)}{rvs\left(B,\phi_{xxx},H\right)\rho\left(B\right)}$$
$$\times\left\langle L_{HAM}\left(B,D,H,C\right)\right\rangle-\left(1-\rho\left(B\right)\right)\left\langle L_{RTA}\left(B,D,H,C\right)\right\rangle \quad . \qquad (7)$$

For the TMC source, we must also determine the effective TMC emissivity. Here we use the following equation

$$\varepsilon_{TMC}\left(B,D,C\right)=\frac{\left\langle L_{TMC}\left(B,D,C\right)\right\rangle_{retrieved}-\left\langle L_{Bkg}\left(B,D,C\right)\right\rangle}{\left\langle L_{TMC}\left(B,D,C\right)\right\rangle-\left\langle L_{Bkg}\left(B,D,C\right)\right\rangle}, \qquad (8)$$

where the retrieved TMC radiance was averaged over HAM sides and

$$\left\langle L_{Bkg}\left(B,D,H,C\right)\right\rangle=rvs\left(B,\phi_{SVS},H\right)\left\langle L_{SVS}\left(B,D,C\right)\right\rangle$$
$$-\frac{rvs\left(B,\phi_{SVS},H\right)-rvs\left(B,\phi_{xxx},H\right)}{\rho_{RTA}\left(B\right)}$$
$$\times\left\langle L_{HAM}\left(B,D,H,C\right)\right\rangle-\left(1-\rho_{RTA}\left(B\right)\right)\left\langle L_{RTA}\left(B,D,H,C\right)\right\rangle \quad , \qquad (9)$$

which was also averaged over HAM sides. The emissivity is then averaged over detectors. This detector averaged emissivity is then extrapolated from the low temperature range to high temperature by means of a linear fit.

## 2.2 High Temperature

For the high temperature range, only data from the TMC source and band M13 were considered. The radiances are calculated as for low temperature; the TMC emissivity is applied to the RSR corrected radiance for the TMC using the following

$$\left\langle L_{TMC}\left(B,D,C\right)\right\rangle_{new}=\varepsilon_{TMC}\left(B,C\right)\left\langle L_{TMC}\left(B,D,C\right)\right\rangle-\left(1-\varepsilon_{TMC}\left(B,C\right)\right)\left\langle L_{Bkg}\left(B,D,C\right)\right\rangle. \qquad (10)$$

This corrected TMC radiance is then substituted into Equation (4). The resulting high temperature delta radiance is used to perform polynomial fitting as in the low temperature region. Here only collects in fixed low gain mode and above $T_{MIN}$ for M13 low gain were used (UAIDs 2002526 – 32). The inverse of the linear term ($1/a_1$) is the radiometric gain of the low gain sector for band M13.

## 3. Specification

The five specifications that are considered in this memo are listed in Table 2 [3,8].

SRV0448 investigates the response characterization. This requirement is accessed using the Radiometric Response Characterization Uncertainty (RRCU), or

$$RRCU=\sqrt{mean_C\left(\Delta_{fit}\right)^2+\sigma_C\left(\Delta_{fit}\right)^2}. \qquad (11)$$

This specification is met if the RRCU is less than 0.1 %. Here $\Delta_{fit}$ is the fractional fitting residual derived from a polynomial fit of dn to $\Delta L_{BCS}$, as defined in Equation (6).

The specification SRV0595 evaluates the response linearity. In this work, SRV0595 is investigated using the Relative Response Non-Linearity (RRNL), or

$$RRNL = \frac{\max_C \left| \Delta_{fit} \times \Delta L_{BCS} \right|}{L_{MAX}}. \quad (12)$$

As this is a measurement of the deviation from linearity, the fitting residual (not the fractional residual) for a linear polynomial fit is used to calculate the RRNL. The VIIRS sensor meets this requirement if the RRNL is less than 1 %. Note that the $L_{MAX}$ used here is normalized to F9, as the EDU data is F9.

The following two requirements address the absolute calibration uncertainty: SRV0545 and SRV0546. The absolute calibration uncertainty includes all the uncertainties associated with the calibration. This is beyond the scope of this work; however, the fit uncertainty contribution to the absolute uncertainty can be analyzed using the Absolute Radiance Difference (ARD), or

$$ARD = 100 \frac{\langle L_{BCS} \rangle_{retrieved} - \langle L_{BCS} \rangle}{\langle L_{BCS} \rangle}. \quad (13)$$

This is just the percent difference between the retrieved and RSR corrected Planck radiances. This requirement is compared against the values listed in Tables 3 and 4 for the specified scene temperatures. However, the data is for the F9 aperture and the specification is normalized to the F6 aperture. As a result, the scene temperatures are converted to F9, shown in Table 5. These requirements are compared to the ARD at the BCS temperature nearest to the F9 scene temperatures.

The final specification (SRV0613) considered here investigates the response uniformity. This particular requirement is assessed by means of the Relative Response Uniformity (RRU), or

$$RRU = \frac{\max_D \left| \langle L_{BCS} \rangle_{retrieved} - \langle L_{BCS} \rangle - mean_D \langle L_{BCS} \rangle_{retrieved} - \langle L_{BCS} \rangle \right|}{NEdL_{spec}}, \quad (14)$$

where the difference between the retrieved radiance and the RSR corrected source radiance is used here. This delta radiance was employed in place of the RSR corrected radiance to avoid the large spectral variation from detector to detector produced in the RSR by the spectral smile of the SPMA [5]. This specification is met if the RRU is less than 1. Note that the $NEdL_{spec}$ has been converted to its F9 value.

## 4. Analysis

### 4.1 Radiometric Gains

The radiometric gains, evaluated using the above procedure, are listed for each individual detector in Table 6 (for the quadratic fit with the RSR correction). Note that all the numbers given here are for the F9 aperture. The I bands have been averaged over subsample and HAM side A is presented. HAM side B produces similar results to HAM side A to within 0.5 % for all bands and detectors using the quadratic fit. Furthermore, the gain variations over detectors are as follows: about 7 % for bands M16B, M16A,

M15, and M12; about 10 % for bands M14, M13 (both hg and lg), and I4; and about 15% for band I5. Figure 1 shows the variation of the radiometric gain as a function of detector for each band (except M13 lg).

The radiometric gains are then averaged over detectors; the results are given in Table 7. As detector 1 for band M14 is Out Of Family (OOF), it was not included in the average. The detector averaged gains were calculated using both quadratic and cubic fits as well as with and without the RSR correction. An increase in fitting level from quadratic to cubic only yields about 1 % difference in the gains. In addition, the results are stable to within 1 % for the RSR correction, except for band M13, which shows a difference of less than 4 %.

The maximum fitting residuals (within the dynamic range) for each level of fitting and each band are also listed. Note that the residual improves substantially for M12, M13 hg, and M14 from quadratic to cubic (the region highlighted in blue). We stress that it is unknown whether a cubic polynomial is a good approximation for the cases considered. Higher order polynomials are more unstable and the fitting residual may result from test artifacts, especially at the low end of the dynamic range.

For comparison, the published Raytheon results for the radiometric gains are also listed in Table 7 [4]. Our results are in good agreement with the Raytheon numbers: about 1 % for bands I4, I5, M12, M16A, and M16B; about 3% for bands M14 and M15; and 4.5 % for band M13 hg. Note that the Raytheon calculation only used the SVS source for the background subtraction.

In addition, the radiometric gains, averaged for odd and even detectors separately, are shown in Table 8 (for the quadratic fit with the RSR correction). There is a 1 – 4 % difference between the averages; this result is particularly clear in Figure 1 for the MWIR bands I4, M12, and M13 hg where the difference is more pronounced.

Figures 2 – 9 show the graphs of dn versus $\Delta L_{BCS}$ for all the TEB bands with the corresponding fractional fitting residuals. All plots show F9 data with the RSR correction. Each figure shows (from top to bottom) the fitting using a linear, quadratic and cubic polynomial. The dynamic range is also marked: $L_{MIN}$ in green, $L_{TYP}$ in blue, and $L_{MAX}$ in red. $L_{MAX}$ is not included on any of the figures because it lies well beyond the range of measured data. The dynamic range requirement was not fully tested here, as no band was close to reaching $L_{MAX}$ for the F9 aperture.

Figure 5 clearly shows that detector 1 for band M14 is OOF (highlighted in red). The fitting residuals are much higher for this detector than any other; as such, it was not included in the detector averaged gain shown in Tables 7 or 8, and will not be included in similar averages for the specifications in the next section.

Bands M12, M13 hg, and M14 all show significant improvement in the fractional fitting residual when increasing the level of fitting from quadratic to cubic; this is seen in Figures 4 and 5 for bands M12 and M13 hg, respectively (highlighted in red). The

improvement occurs at the low end of the dynamic range. The others bands show limited or no improvement when using a cubic polynomial fit. Again we stress that whether a cubic polynomial is good model of the radiometric response here is not known.

### 4.2 Specifications

In Tables 9 – 17, the requirements described above are addressed. Here only HAM side A is presented; HAM side B yields similar results to HAM side A. Also, the results for the I bands are averaged over subsample. In addition, the published Raytheon results are included, where available, to facilitate a comparison [5].

The detector averaged RRCU is listed in Table 9, and the RRCU for the worst case detector is given in Table 10. Both tables show the RRCU results for both quadratic and cubic levels of fitting as well as with and without the RSR correction. The detector averaged RRCU for the quadratic fits fails to meet this specification for the bands I4, M12, M13 hg, and M14 (although M14 is close). The failures are marked in red. However, by implementing a cubic fit, these detector averaged RRCU are substantially reduced for bands M12 and M13 hg (which are now close to meeting the requirement) as well as for M14 (which now meets the specification). I4 does not show any improvement with a change in the fitting level. The RRCU for the worst case detectors show similar trends. Table 11 lists the RRCU for all individual detectors; here the quadratic fits with the RSR correction are shown as well as the cubic fits with the RSR correction for bands M12, M13 hg, and M14. The failures are marked in red.

Figure 10 shows the RRCU as a function of detector for all bands for both quadratic (black) and cubic (red) fits. Note the improvement in RRCU for bands M12, M13 hg, and M14 from increasing the order of the fitting. Also, the RRCU (quadratic fit) are in good agreement with the results of Raytheon [5]. In addition, the improvement from quadratic to cubic fits in the RRCU mirrors the findings of Raytheon [9].

Tables 12 and 13 show the detector averaged RRNL and the RRNL for the worst case detector, respectively. The RRNL are listed for both with and without the RSR correction. Figure 11 shows the RRNL for all bands. Again, there is good agreement with the Raytheon results and all bands meet the specification. Table 14 lists the RRNL for each individual detector; only detector 1 from band M14 fails the specification (marked in red).

The ARD results for the worst case detector are given in Tables 15 and 16, using a quadratic fit for all bands except M12, M13 hg, and M14 for which a cubic fit was used. Those results highlighted in blue are scene temperatures below the F9 $T_{MIN}$ for a particular band. The specifications are marked in green. Those scene temperatures listed in Table 5 below $T_{MIN}$ or above 345 K were not considered. All of the bands met this requirement for the cases that were measured. Additionally, these results are consistent with the published findings of Raytheon [5]. Figures 12 – 19 plot the ARD as a function of detector for each band at the corresponding scene temperatures in Table 5 that are inside the range of measured values.

Listed in Table 17 are the RRU results, using a quadratic fit for all bands except M12, M13 hg, and M14 for which a cubic fit was used. The highlighted numbers are those scene temperatures that lie below $T_{MIN}$ for a given band. The remaining scene temperatures all meet the specification for all bands. This is shown graphically in Figure 20 for all bands as a function of collect (corresponding to the temperatures in Table 1).

## 5. Summary

- Radiometric gains were determined for all TEB bands and are in good agreement with the published findings Raytheon [4].
- The RSR correction is less than 1 % for all bands, except band M13 with less than 4 %.
- HAM side difference in gains is negligible, less than 0.5 %.
- Increasing the degree of polynomial from quadratic to cubic yields only 1 % difference in gains: however, there is substantial improvement in the fitting residual at the low end of the dynamic range for bands M12, M13 hg, and M14.
- Odd – even detector difference of about 1 - 4 % is evident.
- Gain variation over detectors of between 7 – 15 % is observed.
- Band M14, detector 1 is OOF.
- Dynamic range requirement was not verified in this test.
- RRCU does not meet specification (SRV0448) for bands I4, M12, M13 hg, and M14 using a quadratic fit. M12 and M13 hg almost meet the specification when a cubic fit is employed. M14 meets the specification using the cubic fit.
- RRNL meet specification for all bands (SRV0595), except detector 1 from band M14.
- ARD meet specification for all bands (SRV0545 and SRV0546).
- RRU meet specification for all bands (SRV0613).
- Results for RRCU, RRNL, and ARD are all consistent with the published findings of Raytheon [5].

**Acknowledgement**

The sensor test data used in this document was provided by the SBRS testing team. Approaches for data acquisition and data reductions, as well as data extraction tools were also provided by the SBRS. We would like to thank the SBRS team for their support. The data analysis tools were developed by the NICST team, and we would like to extend our gratitude for their valued assistance.

Table 1: EDU RC-05 Part 1 UAIDs with corresponding BCS and TMC temperatures.

| UAID | BCS Temperature (K) | TMC Temperature (K) |
|---|---|---|
| 2002504 | 190.1 | ~ |
| 2002505 | 209.9 | ~ |
| 2002506 | 229.6 | ~ |
| 2002507 | 240.1 | ~ |
| 2002508 | 247.2 | ~ |
| 2002509 | 255.2 | ~ |
| 2002510 | 262.0 | ~ |
| 2002511 | 270.4 | ~ |
| 2002512 | 278.0 | ~ |
| 2002513 | 285.3 | ~ |
| 2002514 | 291.9 | ~ |
| 2002515 | 299.9 | 303.2 |
| 2002516 | 306.8 | 315.2 |
| 2002517 | 314.9 | 326.2 |
| 2002518 | 320.7 | 334.2 |
| 2002519 | 326.8 | 342.2 |
| 2002520 | 331.8 | 348.2 |
| 2002521 | 335.9 | 353.2 |
| 2002522 | 340.0 | 358.2 |
| 2002523 | 345.0 | 364.2 |
| 2002525 | ~ | 378.2 |
| 2002526 | ~ | 513.2 |
| 2002527 | ~ | 563.2 |
| 2002528 | ~ | 608.2 |
| 2002529 | ~ | 638.2 |
| 2002530 | ~ | 663.2 |
| 2002531 | ~ | 688.2 |
| 2002532 | ~ | 718.2 |

Table 2: Specifications addressed by this work [6].

| | |
|---|---|
| SRV0448 | The VIIRS sensor response shall be characterized with an uncertainty better than 0.1% (mean of the ΔL' values plus 1 sigma of the ΔL' values) for the MWIR and LWIR bands. |
| SRV0595 | The nonlinearity (NL) of all spectral bands within a given state shall be less than 0.01 of the response at $L_{MAX}$ / $T_{MAX}$. |
| SRV0545 | For the bands specified as moderate resolution and emissive, the absolute radiometric calibration uncertainty of spectral radiance shall be equal to or less than the percentage specified in TABLE 17. (TABLE 17 is listed as Table 3 in this text.) |
| SRV0546 | For the bands specified as imaging and emissive (TABLE 1), given a uniform scene of brightness temperature of 267 K, the calibration uncertainty of spectral radiance shall be as specified in TABLE 18. (TABLE 18 is listed as Table 4 in this text.) |
| SRV0613 | The calibrated output of all channels within a band shall be matched to the band mean output within the NEdL / NEdT (1 sigma) when viewing a uniform scene. The matching condition shall be met between radiance levels from $L_{MIN}$ to 0.9 $L_{MAX}$. |

Table 3: Absolute radiometric calibration uncertainty of the spectral radiance for moderate resolution emissive bands [3].

| | Scene Temperature (K) | | | | |
|---|---|---|---|---|---|
| Band | 190 | 230 | 270 | 310 | 340 |
| M12 | N/A | 7.00% | 0.70% | 0.70% | 0.70% |
| M13 | N/A | 5.70% | 0.70% | 0.70% | 0.70% |
| M14 | 12.30% | 2.40% | 0.60% | 0.40% | 0.50% |
| M15 | 2.10% | 0.60% | 0.40% | 0.40% | 0.40% |
| M16 | 1.60% | 0.60% | 0.40% | 0.40% | 0.40% |

Table 4: Radiometric calibration uncertainty for imaging emissive bands [3].

| Band | Calibration Uncertainty |
|---|---|
| I4 | 5.00% |
| I5 | 2.50% |

Table 5: Scene temperatures for the SRV0545 and SRV0546 requirements normalized to the F9 aperture.

| | Scene Temperature (K) | | | | | |
|---|---|---|---|---|---|---|
| Band | 190 | 230 | 267 | 270 | 310 | 340 |
| I4 | ~ | ~ | 281.6 | ~ | ~ | ~ |
| I5 | ~ | ~ | 316.4 | ~ | ~ | ~ |
| M12 | ~ | 240.6 | ~ | 284.7 | 329.6 | 363.7 |
| M13 hg | ~ | 241.7 | ~ | 286.2 | 331.6 | 366.1 |
| M14 | 207.5 | 256.1 | ~ | 306.6 | 359.0 | 399.5 |
| M15 | 212.5 | 263.7 | ~ | 317.3 | 373.2 | 416.7 |
| M16 | 215.4 | 268.1 | ~ | 323.4 | 381.3 | 426.3 |

Table 6: Radiometric gains (F9) for TEB bands and HAM side A.

| Detector | I4 | I5 | M12 | M13 hg | M13 lg | M14 | M15 | M16A | M16B |
|---|---|---|---|---|---|---|---|---|---|
| 1 | 469.4 | 47.02 | 769.2 | 326.0 | 1.71 | 139.5 | 99.9 | 112.6 | 116.5 |
| 2 | 455.6 | 47.06 | 764.7 | 322.3 | 1.69 | 111.4 | 98.3 | 115.0 | 115.7 |
| 3 | 471.5 | 47.28 | 789.0 | 336.3 | 1.75 | 105.6 | 99.8 | 112.1 | 114.3 |
| 4 | 467.5 | 47.32 | 773.6 | 327.9 | 1.68 | 105.1 | 99.2 | 113.0 | 115.9 |
| 5 | 482.6 | 47.96 | 797.2 | 338.3 | 1.77 | 107.3 | 100.5 | 113.7 | 114.7 |
| 6 | 485.2 | 47.09 | 771.3 | 321.6 | 1.68 | 109.8 | 94.8 | 115.9 | 117.4 |
| 7 | 494.7 | 47.02 | 797.6 | 334.6 | 1.75 | 108.5 | 101.0 | 112.7 | 117.5 |
| 8 | 480.8 | 46.46 | 776.3 | 318.8 | 1.66 | 107.8 | 99.9 | 116.1 | 118.6 |
| 9 | 502.8 | 48.93 | 799.3 | 335.0 | 1.75 | 103.7 | 98.9 | 111.1 | 115.0 |
| 10 | 504.5 | 48.08 | 780.6 | 322.2 | 1.69 | 105.2 | 98.3 | 112.9 | 112.5 |
| 11 | 500.1 | 49.23 | 789.9 | 336.0 | 1.76 | 102.5 | 99.4 | 111.1 | 115.3 |
| 12 | 494.1 | 48.98 | 789.3 | 317.9 | 1.66 | 107.5 | 96.7 | 113.3 | 112.7 |
| 13 | 505.2 | 48.47 | 783.4 | 322.8 | 1.68 | 109.3 | 94.5 | 112.0 | 112.8 |
| 14 | 498.7 | 48.44 | 763.6 | 308.1 | 1.61 | 106.0 | 96.7 | 112.5 | 111.6 |
| 15 | 506.4 | 48.97 | 766.1 | 316.6 | 1.65 | 100.5 | 97.2 | 109.4 | 111.0 |
| 16 | 494.9 | 48.14 | 747.0 | 305.6 | 1.59 | 98.5 | 93.7 | 108.3 | 107.9 |
| 17 | 505.3 | 48.50 | ~ | ~ | ~ | ~ | ~ | ~ | ~ |
| 18 | 510.7 | 47.22 | ~ | ~ | ~ | ~ | ~ | ~ | ~ |
| 19 | 499.5 | 47.52 | ~ | ~ | ~ | ~ | ~ | ~ | ~ |
| 20 | 495.8 | 46.55 | ~ | ~ | ~ | ~ | ~ | ~ | ~ |
| 21 | 507.2 | 47.48 | ~ | ~ | ~ | ~ | ~ | ~ | ~ |
| 22 | 484.9 | 45.08 | ~ | ~ | ~ | ~ | ~ | ~ | ~ |
| 23 | 491.5 | 46.32 | ~ | ~ | ~ | ~ | ~ | ~ | ~ |
| 24 | 487.5 | 45.70 | ~ | ~ | ~ | ~ | ~ | ~ | ~ |
| 25 | 496.3 | 45.60 | ~ | ~ | ~ | ~ | ~ | ~ | ~ |
| 26 | 489.4 | 43.78 | ~ | ~ | ~ | ~ | ~ | ~ | ~ |
| 27 | 497.9 | 44.10 | ~ | ~ | ~ | ~ | ~ | ~ | ~ |
| 28 | 477.6 | 43.21 | ~ | ~ | ~ | ~ | ~ | ~ | ~ |
| 29 | 495.4 | 42.80 | ~ | ~ | ~ | ~ | ~ | ~ | ~ |
| 30 | 473.9 | 42.72 | ~ | ~ | ~ | ~ | ~ | ~ | ~ |
| 31 | 476.5 | 42.20 | ~ | ~ | ~ | ~ | ~ | ~ | ~ |
| 32 | 472.2 | 41.06 | ~ | ~ | ~ | ~ | ~ | ~ | ~ |

Table 7: Detector averaged radiometric gains (F9) with corresponding maximum fitting residual for HAM side A.

| Band | Raytheon [4] | NICST | | | | | | | |
|---|---|---|---|---|---|---|---|---|---|
| | | Without RSR | | | | With RSR | | | |
| | | Gain (Quadratic) | Fractional Fitting Residual | Gain (Cubic) | Fractional Fitting Residual | Gain (Quadratic) | Fractional Fitting Residual | Gain (Cubic) | Fractional Fitting Residual |
| I4 | 491 | 490.7 | 0.0544 | 493.1 | 0.0257 | 489.9 | 0.0364 | 490.8 | 0.0378 |
| I5 | 46 | 46.04 | 0.0026 | 46.11 | 0.0026 | 46.45 | 0.0025 | 46.51 | 0.0025 |
| M12 | 787 | 784.8 | 0.0476 | 775.6 | 0.0286 | 778.6 | 0.0576 | 768.2 | 0.0212 |
| M13 hg | 338 | 336.1 | 0.0282 | 333.2 | 0.016 | 324.4 | 0.0428 | 320.2 | 0.0091 |
| M13 lg | 1.5 | 1.47 | 0.0018 | 1.45 | 0.0012 | 1.69 | 0.0026 | 1.66 | 0.0012 |
| M14 | 109 | 106.3 | 0.0217 | 106.4 | 0.0032 | 105.9 | 0.0241 | 105.7 | 0.003 |
| M15 | 101 | 97.94 | 0.0015 | 97.78 | 0.0013 | 98.04 | 0.0023 | 98.11 | 0.0015 |
| M16A | 114 | 113.4 | 0.0023 | 112.6 | 0.001 | 112.6 | 0.0011 | 112.5 | 0.0007 |
| M16B | 116 | 115.1 | 0.0017 | 114.3 | 0.0006 | 114.3 | 0.0005 | 114.2 | 0.0005 |

Table 8: Radiometric gains (F9) averaged over the odd and even detectors separately (HAM side A).

| Band | NICST | |
|---|---|---|
| | Odd | Even |
| I4 | 493.9 | 485.8 |
| I5 | 46.84 | 46.06 |
| M12 | 786.5 | 770.8 |
| M13 hg | 330.7 | 318.1 |
| M13 lg | 1.73 | 1.66 |
| M14 | 105.3 | 106.4 |
| M15 | 98.9 | 97.2 |
| M16A | 111.8 | 113.8 |
| M16B | 114.6 | 114.0 |

Table 9: RRCU detector averaged for HAM side A.

| Band | Raytheon [5] | NICST | | | |
|---|---|---|---|---|---|
| | | Without RSR | | With RSR | |
| | | Quadratic | Cubic | Quadratic | Cubic |
| I4 | 0.52% | 0.90% | 0.31% | 0.36% | 0.42% |
| I5 | 0.04% | 0.05% | 0.04% | 0.05% | 0.04% |
| M12 | 1.52% | 1.14% | 0.17% | 1.44% | 0.13% |
| M13 hg | 0.99% | 0.49% | 0.28% | 0.96% | 0.12% |
| M14 | 0.06% | 0.13% | 0.05% | 0.11% | 0.04% |
| M15 | 0.01% | 0.03% | 0.02% | 0.02% | 0.02% |
| M16A | 0.01% | 0.04% | 0.02% | 0.02% | 0.01% |
| M16B | 0.01% | 0.04% | 0.02% | 0.02% | 0.01% |

Table 10: RRCU worst case detector for HAM side A.

| Band | Raytheon [5] | NICST | | | |
|---|---|---|---|---|---|
| | | Without RSR | | With RSR | |
| | | Quadratic | Cubic | Quadratic | Cubic |
| I4 | 0.71% | 1.43% | 0.67% | 0.98% | 1.02% |
| I5 | 0.06% | 0.10% | 0.08% | 0.10% | 0.09% |
| M12 | 1.63% | 1.37% | 0.83% | 1.67% | 0.63% |
| M13 hg | 1.00% | 0.90% | 0.49% | 1.30% | 0.30% |
| M14 | 0.08% | 0.59% | 0.14% | 0.66% | 0.13% |
| M15 | 0.02% | 0.05% | 0.04% | 0.07% | 0.05% |
| M16A | 0.03% | 0.06% | 0.03% | 0.03% | 0.03% |
| M16B | 0.02% | 0.05% | 0.02% | 0.02% | 0.02% |

Table 11: RRCU for each detector and HAM side A.

| Detector | I4 | I5 | M12 | | M13 hg | | M14 | | M15 | M16A | M16B |
|---|---|---|---|---|---|---|---|---|---|---|---|
| | | | Quad | Cubic | Quad | Cubic | Quad | Cubic | | | |
| 1 | 0.27 | 0.035 | 1.27 | 0.067 | 0.90 | 0.14 | 38.0 | 25.2 | 0.014 | 0.021 | 0.022 |
| 2 | 0.24 | 0.039 | 1.29 | 0.061 | 1.01 | 0.11 | 0.030 | 0.029 | 0.020 | 0.012 | 0.015 |
| 3 | 0.36 | 0.039 | 1.55 | 0.19 | 0.98 | 0.086 | 0.037 | 0.024 | 0.016 | 0.012 | 0.010 |
| 4 | 0.27 | 0.057 | 1.26 | 0.066 | 1.30 | 0.30 | 0.030 | 0.030 | 0.021 | 0.033 | 0.019 |
| 5 | 0.49 | 0.044 | 1.51 | 0.085 | 0.91 | 0.11 | 0.045 | 0.024 | 0.013 | 0.013 | 0.014 |
| 6 | 0.40 | 0.053 | 1.36 | 0.085 | 0.80 | 0.20 | 0.040 | 0.026 | 0.020 | 0.011 | 0.017 |
| 7 | 0.26 | 0.036 | 1.48 | 0.034 | 0.90 | 0.11 | 0.053 | 0.079 | 0.019 | 0.028 | 0.011 |
| 8 | 0.38 | 0.090 | 1.50 | 0.057 | 0.89 | 0.12 | 0.026 | 0.028 | 0.020 | 0.011 | 0.009 |
| 9 | 0.29 | 0.038 | 1.59 | 0.097 | 0.97 | 0.079 | 0.046 | 0.032 | 0.012 | 0.008 | 0.018 |
| 10 | 0.42 | 0.028 | 1.62 | 0.12 | 0.94 | 0.10 | 0.13 | 0.13 | 0.016 | 0.025 | 0.018 |
| 11 | 0.49 | 0.054 | 1.67 | 0.15 | 0.98 | 0.056 | 0.16 | 0.067 | 0.016 | 0.014 | 0.017 |
| 12 | 0.31 | 0.043 | 0.49 | 0.63 | 0.87 | 0.14 | 0.14 | 0.059 | 0.058 | 0.019 | 0.017 |
| 13 | 0.30 | 0.074 | 1.64 | 0.11 | 1.03 | 0.041 | 0.20 | 0.042 | 0.073 | 0.014 | 0.018 |
| 14 | 0.28 | 0.040 | 1.62 | 0.14 | 0.90 | 0.10 | 0.03 | 0.029 | 0.030 | 0.016 | 0.018 |
| 15 | 0.23 | 0.052 | 1.60 | 0.12 | 1.05 | 0.089 | 0.033 | 0.018 | 0.014 | 0.013 | 0.019 |
| 16 | 0.23 | 0.039 | 1.57 | 0.11 | 0.92 | 0.10 | 0.66 | 0.057 | 0.022 | 0.011 | 0.012 |
| 17 | 0.33 | 0.028 | ~ | ~ | ~ | ~ | ~ | ~ | ~ | ~ | ~ |
| 18 | 0.34 | 0.046 | ~ | ~ | ~ | ~ | ~ | ~ | ~ | ~ | ~ |
| 19 | 0.48 | 0.029 | ~ | ~ | ~ | ~ | ~ | ~ | ~ | ~ | ~ |
| 20 | 0.37 | 0.027 | ~ | ~ | ~ | ~ | ~ | ~ | ~ | ~ | ~ |
| 21 | 0.42 | 0.074 | ~ | ~ | ~ | ~ | ~ | ~ | ~ | ~ | ~ |
| 22 | 0.26 | 0.041 | ~ | ~ | ~ | ~ | ~ | ~ | ~ | ~ | ~ |
| 23 | 0.40 | 0.041 | ~ | ~ | ~ | ~ | ~ | ~ | ~ | ~ | ~ |
| 24 | 0.26 | 0.055 | ~ | ~ | ~ | ~ | ~ | ~ | ~ | ~ | ~ |
| 25 | 0.47 | 0.037 | ~ | ~ | ~ | ~ | ~ | ~ | ~ | ~ | ~ |
| 26 | 0.23 | 0.038 | ~ | ~ | ~ | ~ | ~ | ~ | ~ | ~ | ~ |
| 27 | 0.38 | 0.042 | ~ | ~ | ~ | ~ | ~ | ~ | ~ | ~ | ~ |
| 28 | 0.33 | 0.042 | ~ | ~ | ~ | ~ | ~ | ~ | ~ | ~ | ~ |
| 29 | 0.47 | 0.062 | ~ | ~ | ~ | ~ | ~ | ~ | ~ | ~ | ~ |
| 30 | 0.41 | 0.053 | ~ | ~ | ~ | ~ | ~ | ~ | ~ | ~ | ~ |
| 31 | 0.64 | 0.044 | ~ | ~ | ~ | ~ | ~ | ~ | ~ | ~ | ~ |
| 32 | 0.43 | 0.043 | ~ | ~ | ~ | ~ | ~ | ~ | ~ | ~ | ~ |

Table 12: RRNL detector averaged for HAM side A.

| Band | Raytheon [5] | NICST Without RSR Linear | NICST With RSR Linear |
|---|---|---|---|
| I4 | 0.03% | 0.02% | 0.04% |
| I5 | 0.02% | 0.03% | 0.03% |
| M12 | 0.03% | 0.04% | 0.03% |
| M13 hg | 0.20% | 0.25% | 0.19% |
| M14 | 0.15% | 0.21% | 0.17% |
| M15 | 0.02% | 0.03% | 0.03% |
| M16A | 0.02% | 0.04% | 0.02% |
| M16B | 0.02% | 0.04% | 0.02% |

Table 13: RRNL worst case detector for HAM side A.

| Band | Raytheon [5] | NICST Without RSR Linear | NICST With RSR Linear |
|---|---|---|---|
| I4 | 0.05% | 0.03% | 0.06% |
| I5 | 0.03% | 0.04% | 0.05% |
| M12 | 0.03% | 0.05% | 0.07% |
| M13 hg | 0.21% | 0.28% | 0.23% |
| M14 | 0.15% | 0.41% | 0.37% |
| M15 | 0.02% | 0.14% | 0.11% |
| M16A | 0.02% | 0.05% | 0.03% |
| M16B | 0.02% | 0.04% | 0.04% |

Table 14: RRNL for each detector and HAM side A.

| Detector | I4 | I5 | M12 | M13 hg | M14 | M15 | M16A | M16B |
|---|---|---|---|---|---|---|---|---|
| 1 | 0.032 | 0.028 | 0.028 | 0.21 | 11.9 | 0.010 | 0.013 | 0.020 |
| 2 | 0.030 | 0.037 | 0.030 | 0.20 | 0.12 | 0.017 | 0.017 | 0.026 |
| 3 | 0.035 | 0.026 | 0.039 | 0.22 | 0.17 | 0.019 | 0.021 | 0.022 |
| 4 | 0.034 | 0.041 | 0.032 | 0.070 | 0.17 | 0.022 | 0.029 | 0.027 |
| 5 | 0.037 | 0.036 | 0.032 | 0.23 | 0.15 | 0.023 | 0.019 | 0.023 |
| 6 | 0.027 | 0.044 | 0.031 | 0.20 | 0.18 | 0.11 | 0.024 | 0.024 |
| 7 | 0.033 | 0.027 | 0.030 | 0.22 | 0.31 | 0.030 | 0.020 | 0.016 |
| 8 | 0.029 | 0.039 | 0.030 | 0.20 | 0.12 | 0.011 | 0.016 | 0.019 |
| 9 | 0.030 | 0.034 | 0.030 | 0.22 | 0.15 | 0.018 | 0.015 | 0.022 |
| 10 | 0.031 | 0.036 | 0.031 | 0.20 | 0.21 | 0.019 | 0.021 | 0.035 |
| 11 | 0.035 | 0.031 | 0.032 | 0.21 | 0.083 | 0.020 | 0.016 | 0.019 |
| 12 | 0.036 | 0.037 | 0.070 | 0.19 | 0.20 | 0.035 | 0.015 | 0.022 |
| 13 | 0.039 | 0.037 | 0.033 | 0.21 | 0.13 | 0.030 | 0.014 | 0.015 |
| 14 | 0.037 | 0.036 | 0.034 | 0.17 | 0.13 | 0.061 | 0.015 | 0.023 |
| 15 | 0.040 | 0.041 | 0.034 | 0.20 | 0.16 | 0.020 | 0.012 | 0.018 |
| 16 | 0.037 | 0.036 | 0.039 | 0.16 | 0.37 | 0.061 | 0.017 | 0.025 |
| 17 | 0.038 | 0.026 | ~ | ~ | ~ | ~ | ~ | ~ |
| 18 | 0.037 | 0.035 | ~ | ~ | ~ | ~ | ~ | ~ |
| 19 | 0.041 | 0.030 | ~ | ~ | ~ | ~ | ~ | ~ |
| 20 | 0.044 | 0.029 | ~ | ~ | ~ | ~ | ~ | ~ |
| 21 | 0.045 | 0.039 | ~ | ~ | ~ | ~ | ~ | ~ |
| 22 | 0.046 | 0.037 | ~ | ~ | ~ | ~ | ~ | ~ |
| 23 | 0.048 | 0.025 | ~ | ~ | ~ | ~ | ~ | ~ |
| 24 | 0.045 | 0.042 | ~ | ~ | ~ | ~ | ~ | ~ |
| 25 | 0.049 | 0.029 | ~ | ~ | ~ | ~ | ~ | ~ |
| 26 | 0.045 | 0.029 | ~ | ~ | ~ | ~ | ~ | ~ |
| 27 | 0.051 | 0.030 | ~ | ~ | ~ | ~ | ~ | ~ |
| 28 | 0.056 | 0.028 | ~ | ~ | ~ | ~ | ~ | ~ |
| 29 | 0.048 | 0.045 | ~ | ~ | ~ | ~ | ~ | ~ |
| 30 | 0.050 | 0.031 | ~ | ~ | ~ | ~ | ~ | ~ |
| 31 | 0.051 | 0.027 | ~ | ~ | ~ | ~ | ~ | ~ |
| 32 | 0.052 | 0.020 | ~ | ~ | ~ | ~ | ~ | ~ |

Table 15: ARD worst case detector for bands I4, M12, M13 hg, and M14.

| BCS Temp | I4 | | M12 | | M13 hg | | M14 | |
|---|---|---|---|---|---|---|---|---|
| | Raytheon [5] | NICST | Raytheon [5] | NICST | Raytheon [5] | NICST | Raytheon [5] | NICST |
| 190.1 | 96.7 | 408.7 | 838.3 | 961.4 | 355.4 | 442.1 | 0.663 | 4.183 |
| 209.9 | 13.51 | 53.50 | 124.5 | 127.4 | 53.71 | 68.83 | 0.226 | 1.556 |
| 229.6 | 2.810 | 48.50 | 24.11 | 24.09 | 11.85 | 14.94 | 0.127 | 0.207 |
| 240.1 | 1.108 | 2.819 | 10.00 | 10.34 | 5.675 | 6.674 | 0.079 | 0.082 |
| 247.2 | 0.659 | 1.429 | 5.516 | 5.695 | 3.363 | 4.245 | 0.022 | 0.246 |
| 255.2 | 0.428 | 0.765 | 2.914 | 2.923 | 1.629 | 2.044 | 0.033 | 0.163 |
| 262 | 0.155 | 0.673 | 1.356 | 1.391 | 0.798 | 1.321 | 0.019 | 0.117 |
| 270.4 | 0.304 | 0.540 | 0.488 | 0.555 | 0.403 | 0.664 | 0.049 | 0.242 |
| 278 | 0.193 | 0.343 | 0.165 | 0.162 | 0.079 | 0.180 | 0.076 | 0.131 |
| 285.3 | 0.086 | 0.144 | 0.346 | 0.375 | 0.287 | 0.330 | 0.016 | 0.038 |
| 291.9 | 0.086 | 0.159 | 0.394 | 0.410 | 0.369 | 0.475 | 0.016 | 0.035 |
| 299.9 | 0.062 | 0.125 | 0.421 | 0.440 | 0.317 | 0.447 | 0.006 | 0.062 |
| 306.8 | 0.085 | 0.115 | 0.294 | 0.300 | 0.272 | 0.437 | 0.006 | 0.032 |
| 314.9 | 0.040 | 0.068 | 0.158 | 0.183 | 0.151 | 0.240 | 0.019 | 0.079 |
| 320.7 | 0.041 | 0.058 | 0.070 | 0.174 | 0.031 | 0.057 | 0.019 | 0.036 |
| 326.8 | 0.012 | 0.033 | 0.033 | 0.430 | 0.110 | 0.114 | 0.024 | 0.048 |
| 331.8 | 0.031 | 0.039 | 0.109 | 0.140 | 0.231 | 0.188 | 0.016 | 0.025 |
| 335.9 | 0.045 | 0.042 | 0.133 | 0.133 | 0.093 | 0.163 | 0.005 | 0.028 |
| 340 | 0.025 | 0.031 | 0.077 | 0.105 | 0.044 | 0.044 | 0.013 | 0.026 |
| 345 | 0.027 | 0.031 | 0.114 | 0.115 | 0.090 | 0.145 | 0.013 | 0.037 |

Table 16: ARD worst case detector for bands I5, M15, M16A, and M16B.

| BCS Temp | M15 | | I5 | | M16A | | M16B | |
|---|---|---|---|---|---|---|---|---|
| | Raytheon [5] | NICST | 5 | NICST | Raytheon [5] | NICST | Raytheon [5] | NICST |
| 190.1 | 0.598 | 2.773 | 1.419 | 1.584 | 0.287 | 0.438 | 0.261 | 0.682 |
| 209.9 | 0.203 | 1.092 | 0.523 | 0.969 | 0.094 | 0.112 | 0.081 | 0.196 |
| 229.6 | 0.048 | 0.191 | 0.127 | 0.175 | 0.078 | 0.103 | 0.050 | 0.048 |
| 240.1 | 0.048 | 0.115 | 0.107 | 0.166 | 0.044 | 0.030 | 0.040 | 0.036 |
| 247.2 | 0.028 | 0.025 | 0.153 | 0.212 | 0.031 | 0.046 | 0.017 | 0.044 |
| 255.2 | 0.028 | 0.079 | 0.051 | 0.127 | 0.021 | 0.040 | 0.015 | 0.046 |
| 262 | 0.027 | 0.052 | 0.087 | 0.138 | 0.013 | 0.028 | 0.023 | 0.026 |
| 270.4 | 0.015 | 0.059 | 0.119 | 0.127 | 0.029 | 0.044 | 0.045 | 0.041 |
| 278 | 0.034 | 0.033 | 0.048 | 0.111 | 0.036 | 0.038 | 0.025 | 0.042 |
| 285.3 | 0.026 | 0.053 | 0.045 | 0.074 | 0.015 | 0.018 | 0.014 | 0.018 |
| 291.9 | 0.011 | 0.029 | 0.048 | 0.110 | 0.015 | 0.018 | 0.015 | 0.021 |
| 299.9 | 0.016 | 0.042 | 0.042 | 0.102 | 0.025 | 0.029 | 0.010 | 0.024 |
| 306.8 | 0.019 | 0.039 | 0.052 | 0.072 | 0.019 | 0.031 | 0.015 | 0.021 |
| 314.9 | 0.006 | 0.030 | 0.036 | 0.071 | 0.018 | 0.019 | 0.014 | 0.021 |
| 320.7 | 0.010 | 0.042 | 0.034 | 0.052 | 0.007 | 0.024 | 0.011 | 0.012 |
| 326.8 | 0.006 | 0.036 | 0.033 | 0.052 | 0.009 | 0.015 | 0.021 | 0.020 |
| 331.8 | 0.005 | 0.028 | 0.031 | 0.047 | 0.012 | 0.012 | 0.008 | 0.011 |
| 335.9 | 0.004 | 0.014 | 0.051 | 0.077 | 0.010 | 0.010 | 0.010 | 0.014 |
| 340 | 0.011 | 0.015 | 0.017 | 0.058 | 0.011 | 0.012 | 0.017 | 0.014 |
| 345 | 0.007 | 0.031 | 0.014 | 0.033 | 0.007 | 0.010 | 0.009 | 0.011 |

Table 17: RRU worst case detector for HAM side A.

| BCS Temp | I4 | I5 | M12 | M13 hg | M14 | M15 | M16A | M16B |
|---|---|---|---|---|---|---|---|---|
| 190.1 | 0.022 | 0.127 | 0.099 | 0.150 | 0.817 | 1.480 | 0.168 | 0.351 |
| 209.9 | 0.020 | 0.101 | 0.272 | 0.191 | 0.570 | 1.050 | 0.135 | 0.218 |
| 229.6 | 0.017 | 0.038 | 0.145 | 0.142 | 0.194 | 0.315 | 0.170 | 0.108 |
| 240.1 | 0.017 | 0.038 | 0.136 | 0.135 | 0.169 | 0.233 | 0.100 | 0.102 |
| 247.2 | 0.012 | 0.060 | 0.148 | 0.079 | 0.342 | 0.070 | 0.122 | 0.130 |
| 255.2 | 0.013 | 0.044 | 0.111 | 0.070 | 0.229 | 0.155 | 0.139 | 0.133 |
| 262.0 | 0.017 | 0.054 | 0.068 | 0.042 | 0.275 | 0.198 | 0.110 | 0.116 |
| 270.4 | 0.012 | 0.063 | 0.021 | 0.079 | 0.670 | 0.540 | 0.197 | 0.120 |
| 278.0 | 0.018 | 0.059 | 0.034 | 0.073 | 0.335 | 0.221 | 0.115 | 0.159 |
| 285.3 | 0.011 | 0.052 | 0.109 | 0.043 | 0.153 | 0.306 | 0.118 | 0.105 |
| 291.9 | 0.021 | 0.075 | 0.175 | 0.115 | 0.174 | 0.211 | 0.134 | 0.122 |
| 299.9 | 0.020 | 0.080 | 0.214 | 0.074 | 0.223 | 0.385 | 0.144 | 0.151 |
| 306.8 | 0.019 | 0.058 | 0.148 | 0.134 | 0.209 | 0.269 | 0.186 | 0.135 |
| 314.9 | 0.012 | 0.058 | 0.146 | 0.058 | 0.456 | 0.274 | 0.144 | 0.111 |
| 320.7 | 0.009 | 0.058 | 0.290 | 0.081 | 0.270 | 0.321 | 0.206 | 0.130 |
| 326.8 | 0.017 | 0.057 | 0.162 | 0.084 | 0.383 | 0.375 | 0.169 | 0.196 |
| 331.8 | 0.016 | 0.049 | 0.031 | 0.061 | 0.212 | 0.297 | 0.141 | 0.128 |
| 335.9 | 0.014 | 0.070 | 0.150 | 0.079 | 0.187 | 0.152 | 0.078 | 0.156 |
| 340.0 | 0.012 | 0.073 | 0.237 | 0.097 | 0.219 | 0.183 | 0.111 | 0.107 |
| 345.0 | 0.011 | 0.041 | 0.155 | 0.058 | 0.319 | 0.445 | 0.074 | 0.130 |

Figure 1: Radiometric gains as a function of detector for all bands (except M13 lg), HAM side A, and subsample 1.

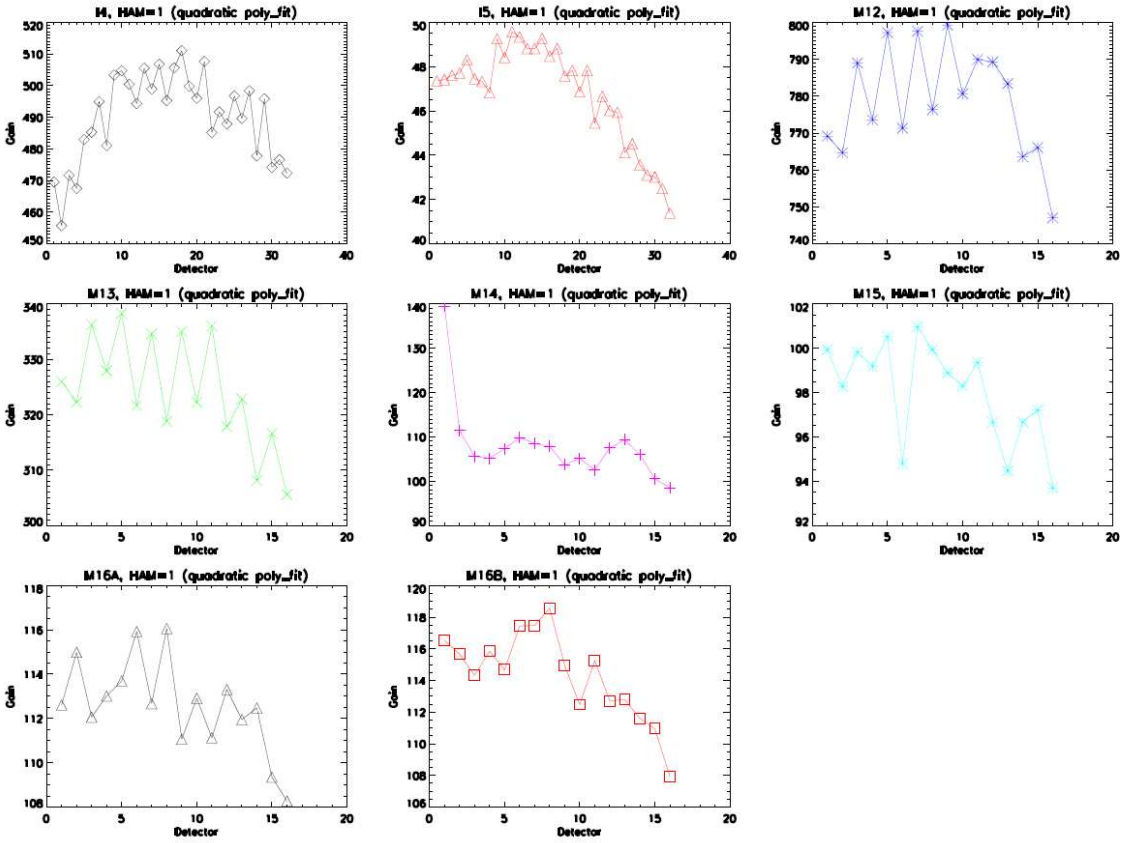

Figure 2: dn versus $\Delta L_{BCS}$ for I4, subsample 1 and HAM side A with corresponding fitting residual.

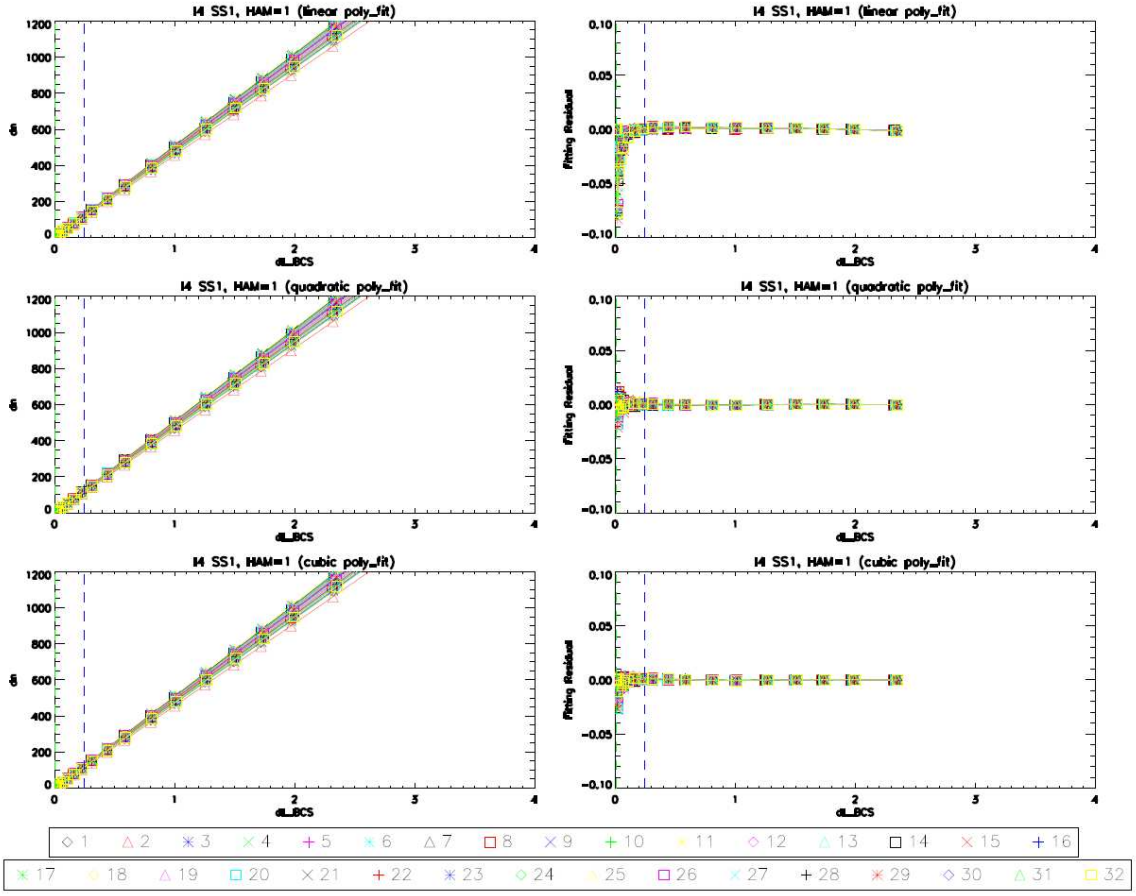

Figure 3: dn versus $\Delta L_{BCS}$ for I5, subsample 1 and HAM side A with corresponding fitting residuals.

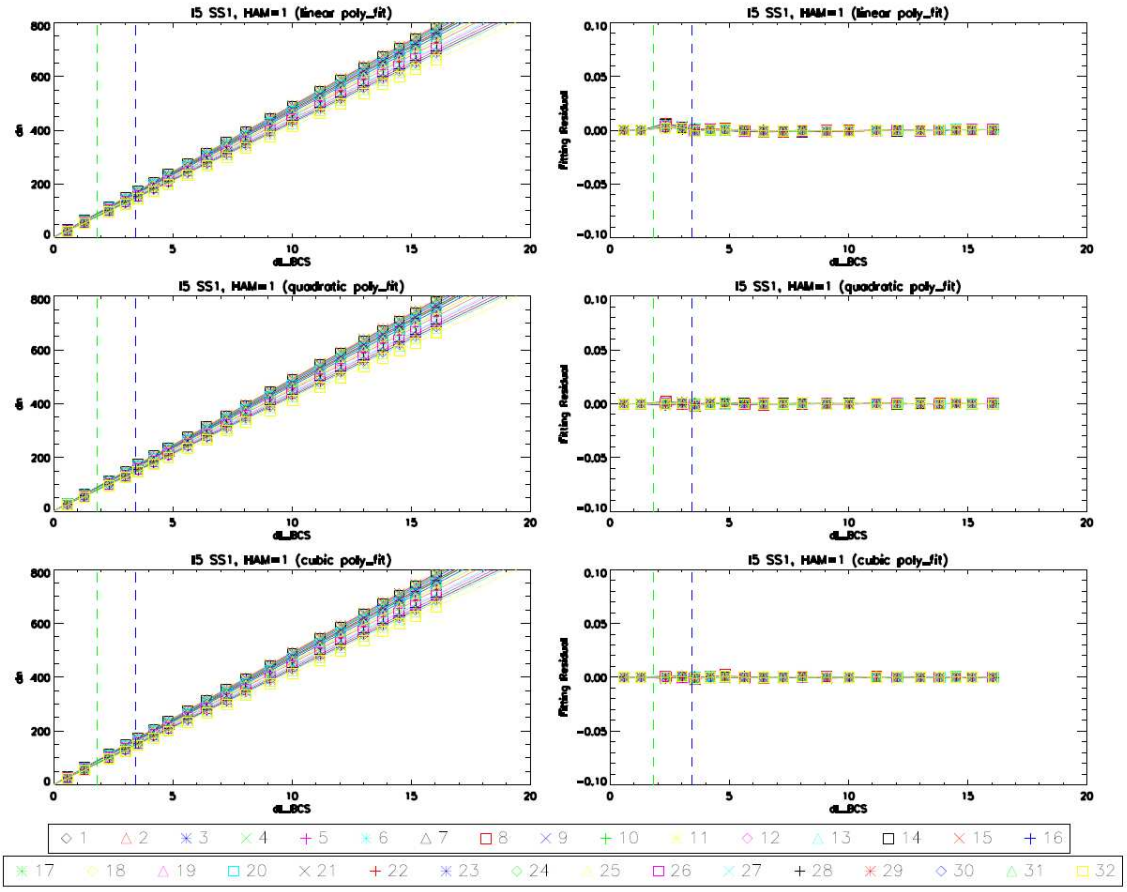

Figure 4: dn versus $\Delta L_{BCS}$ for M12, HAM side A with corresponding fitting residuals.

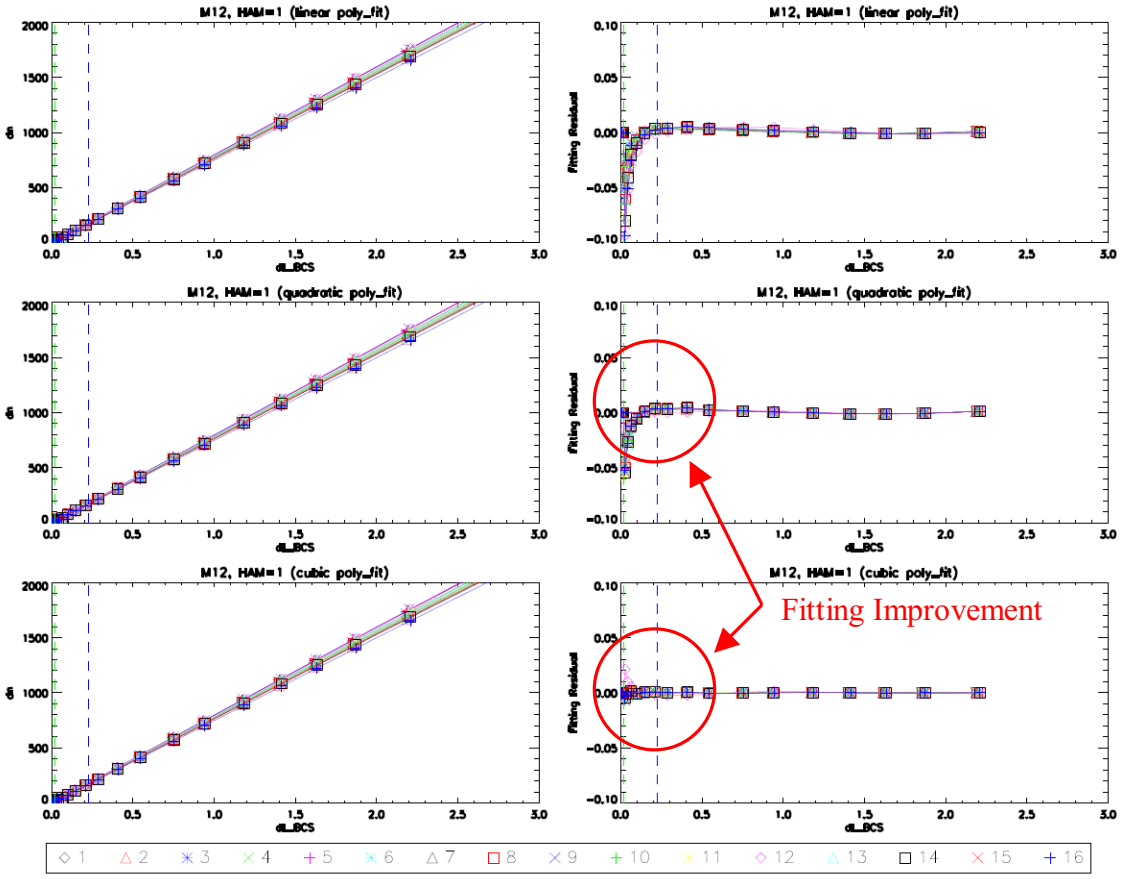

Figure 5: dn versus $\Delta L_{BCS}$ for M13 hg, HAM side A with corresponding fitting residuals.

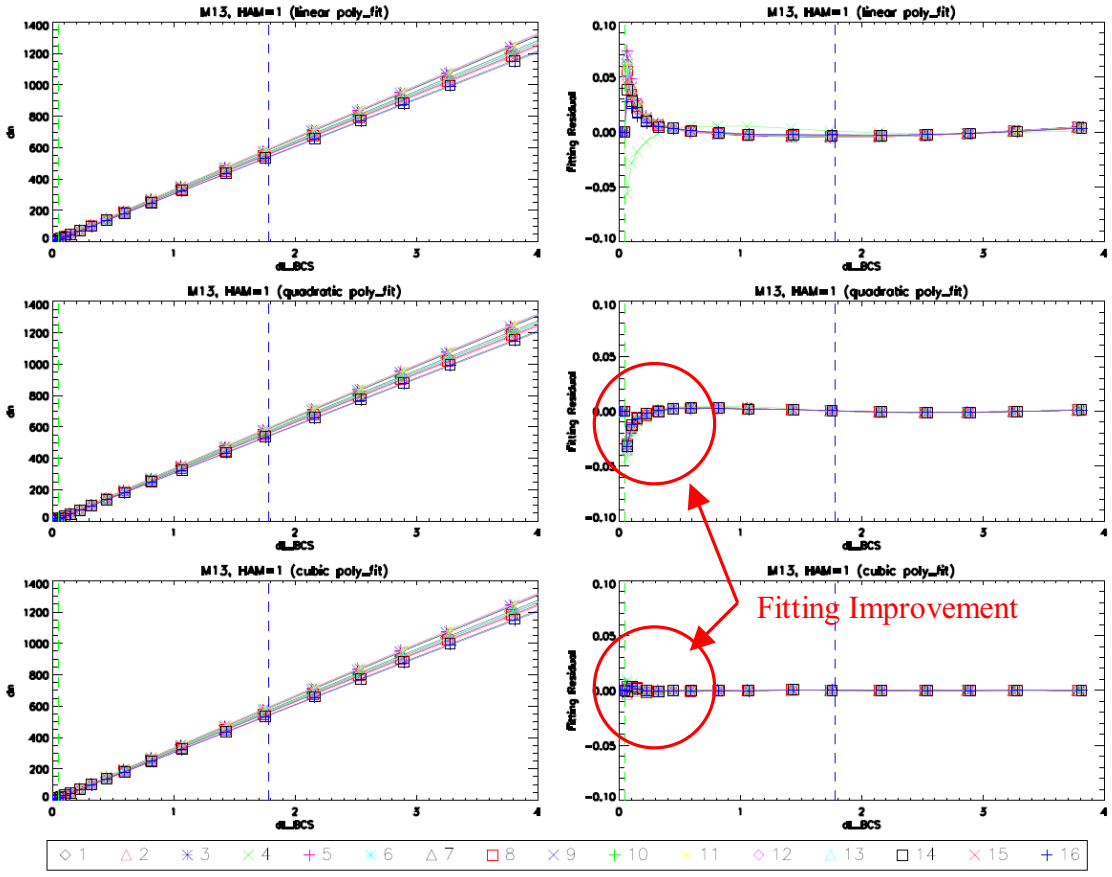

Figure 6: dn versus $\Delta L_{BCS}$ for M14, HAM side A with corresponding fitting residuals.

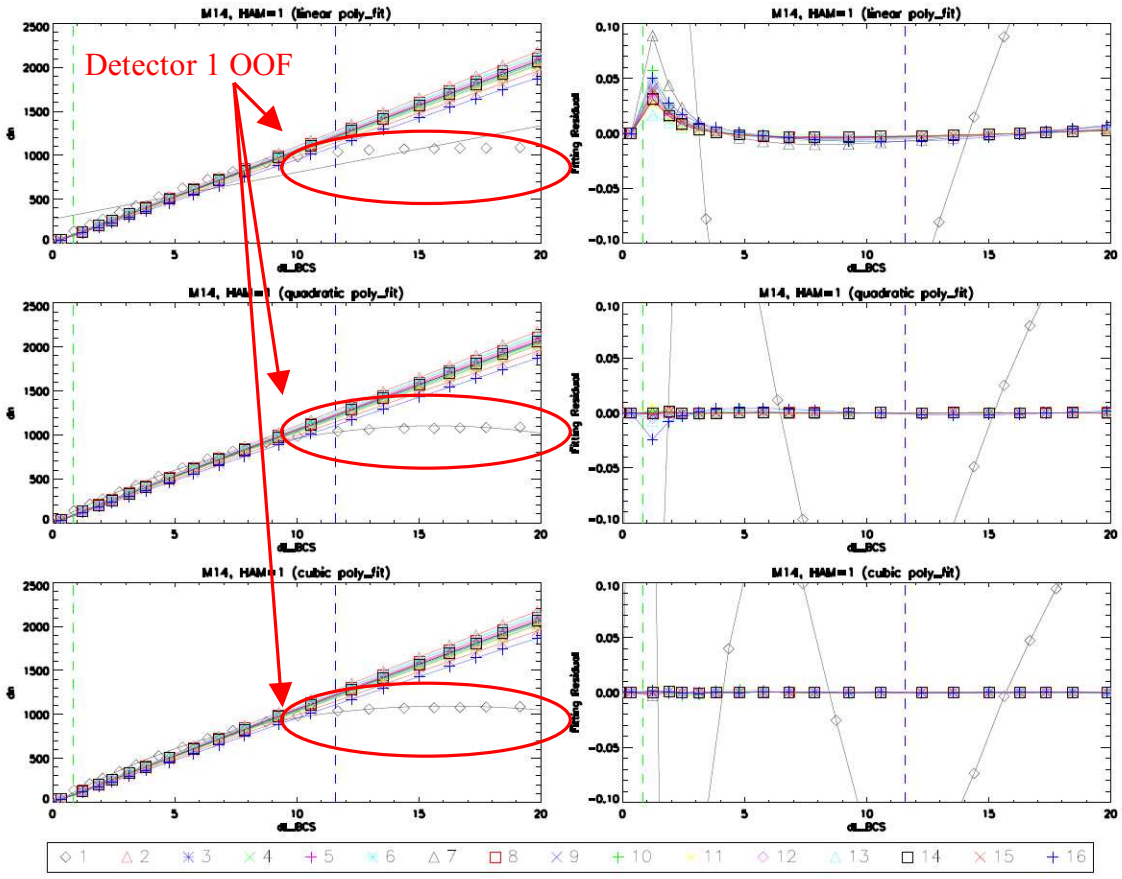

Figure 7: dn versus $\Delta L_{BCS}$ for M15, HAM side A with corresponding fitting residuals.

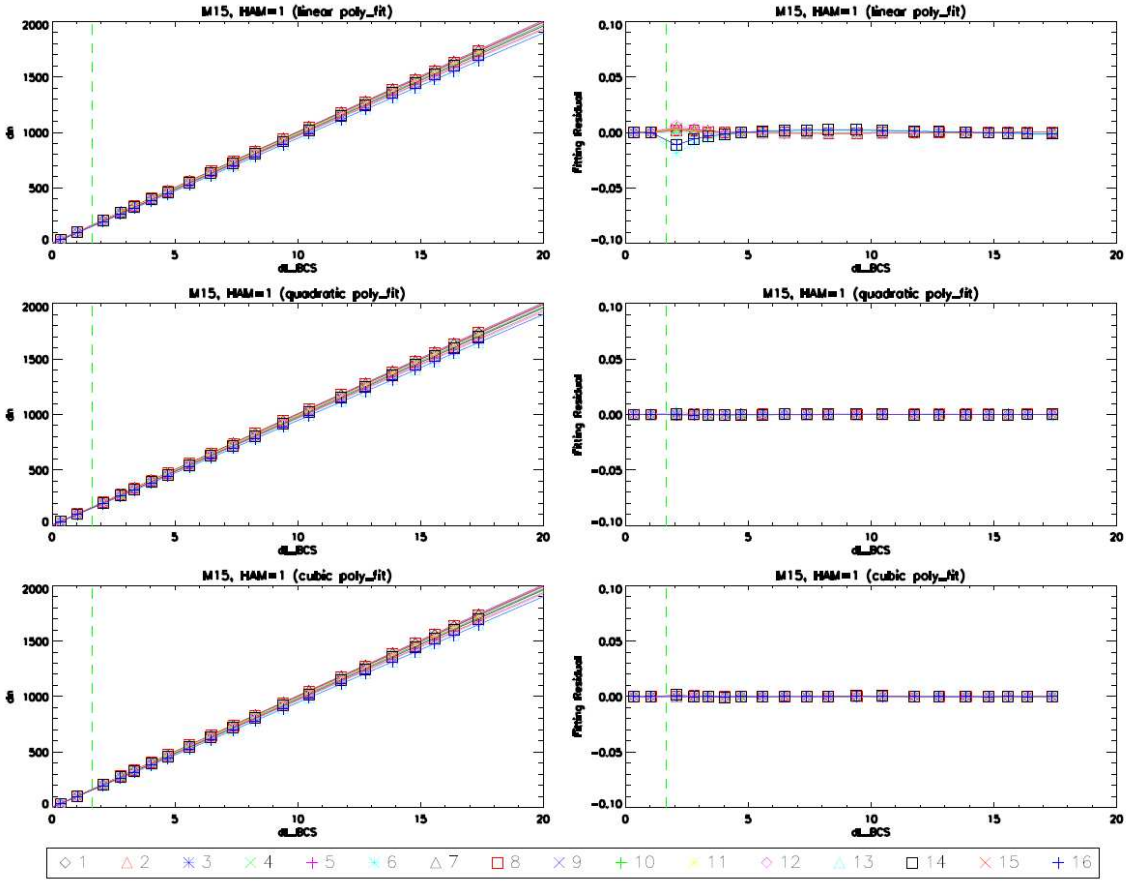

Figure 8: dn versus $\Delta L_{BCS}$ for M16A, HAM side A with corresponding fitting residuals.

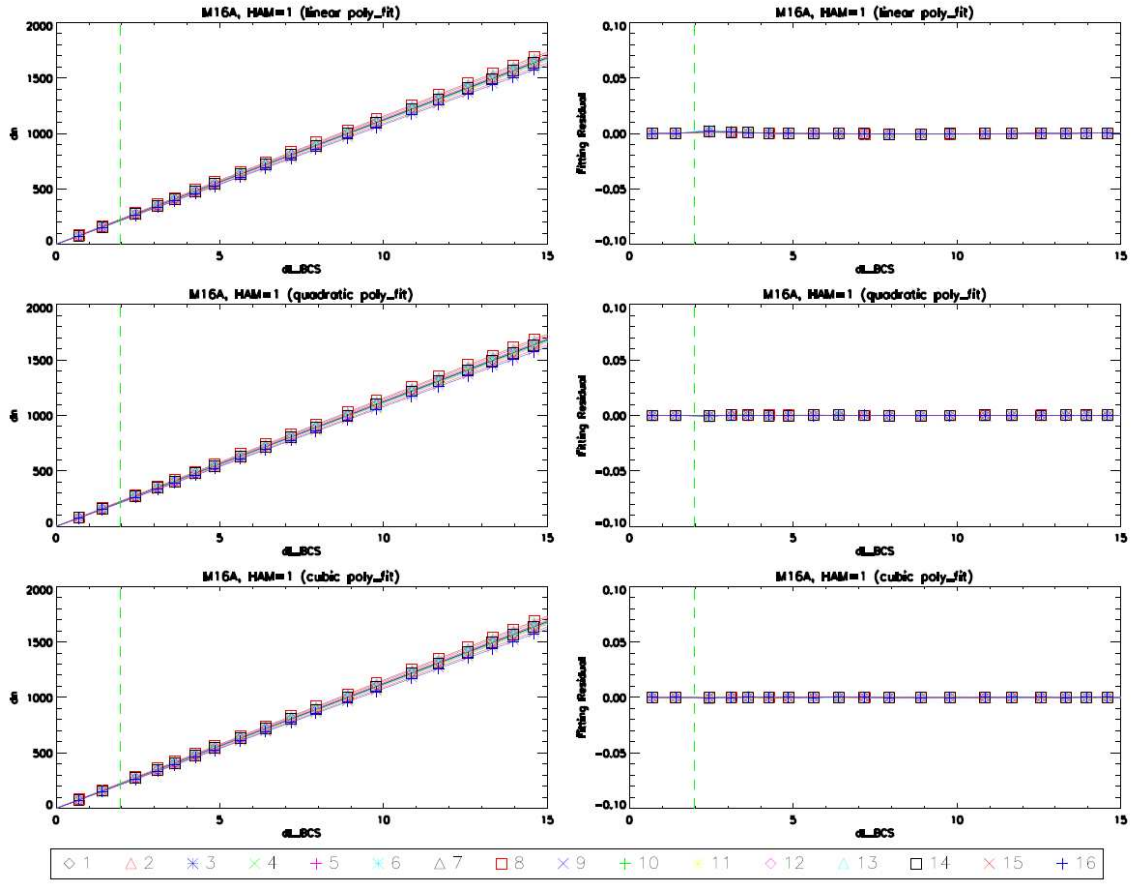

Figure 9: dn versus $\Delta L_{BCS}$ for M16B, HAM side A with corresponding fitting residuals.

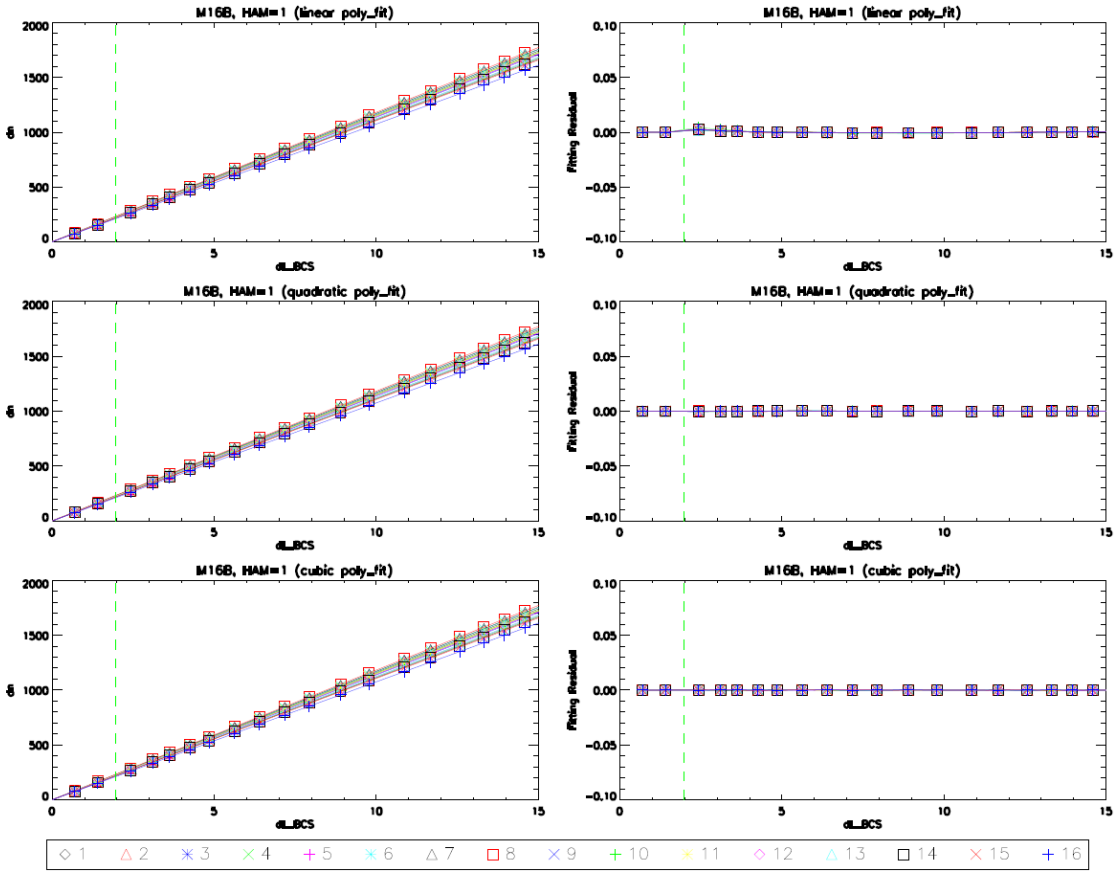

Figure 10: RRCU for both quadratic and cubic fits (black and red, respectively).

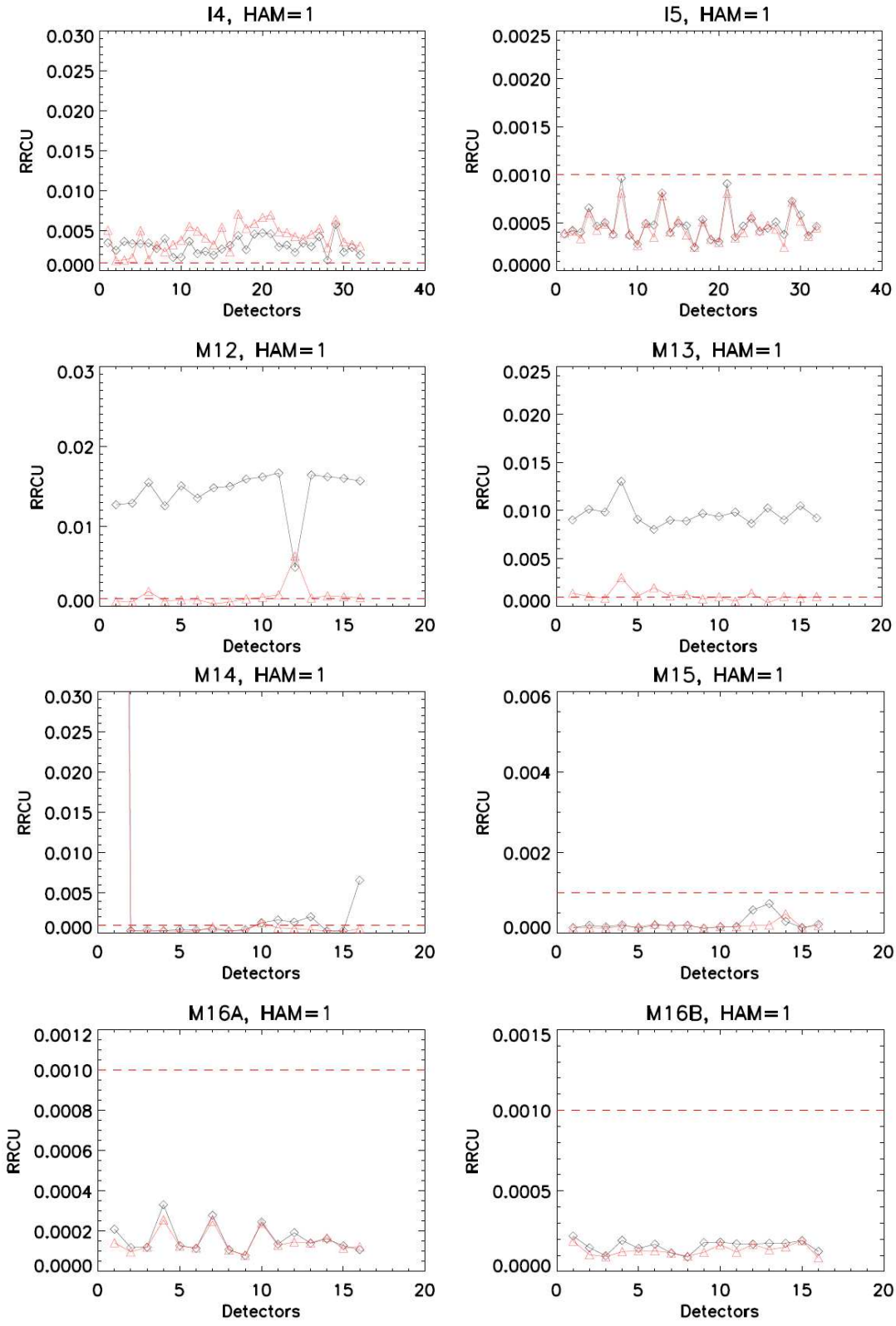

Figure 11: RRNL for HAM side A.

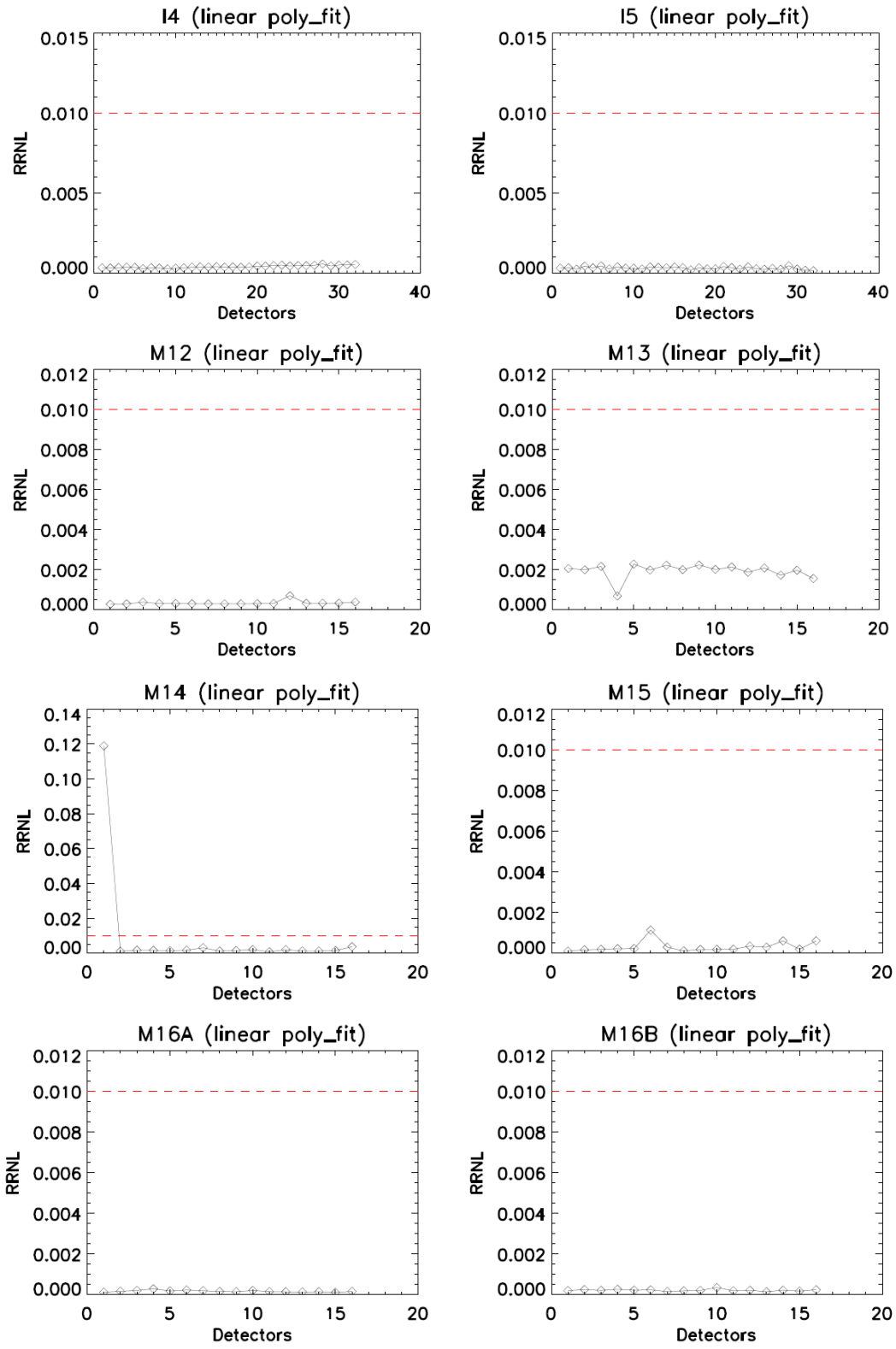

Figure 12: I4 ARD for HAM side A, subsample 1.

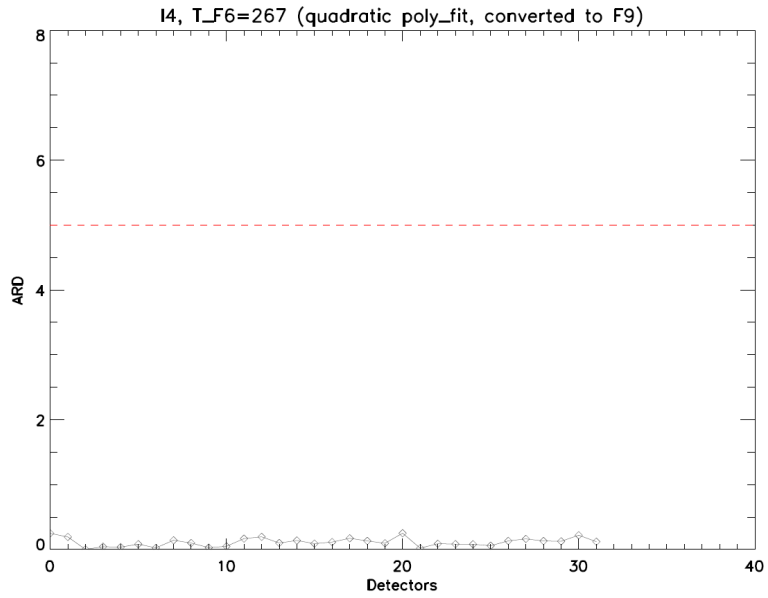


Figure 13: I5 ARD for HAM side A, subsample 1.

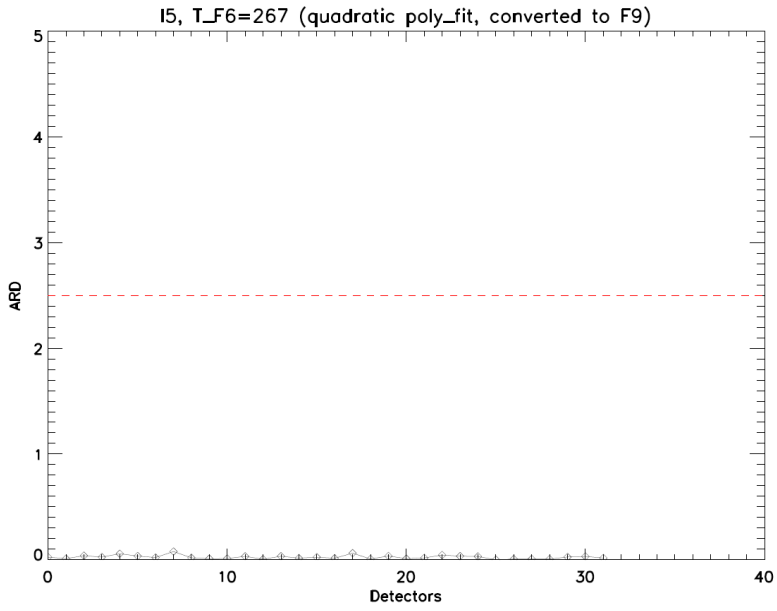

Figure 14: M12 ARD for HAM side A.

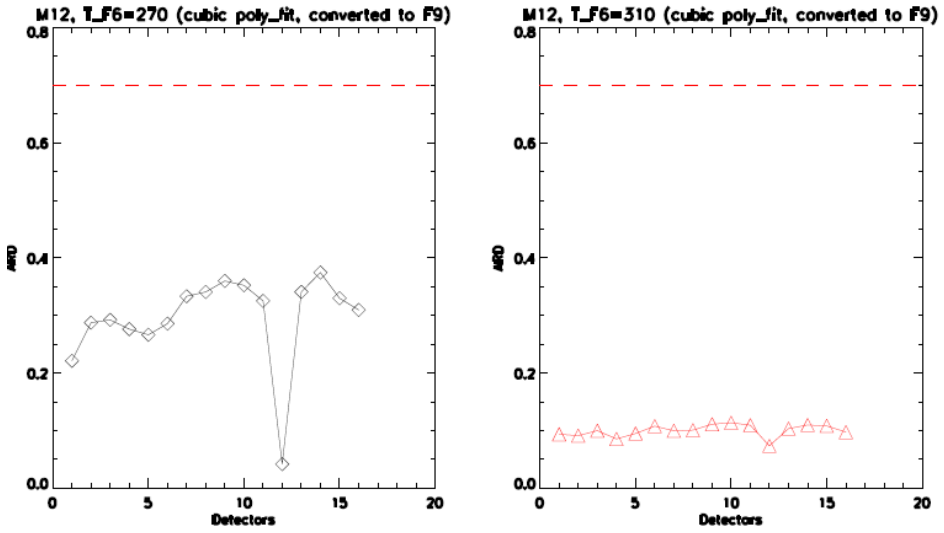


Figure 15: M13 hg ARD for HAM side A.

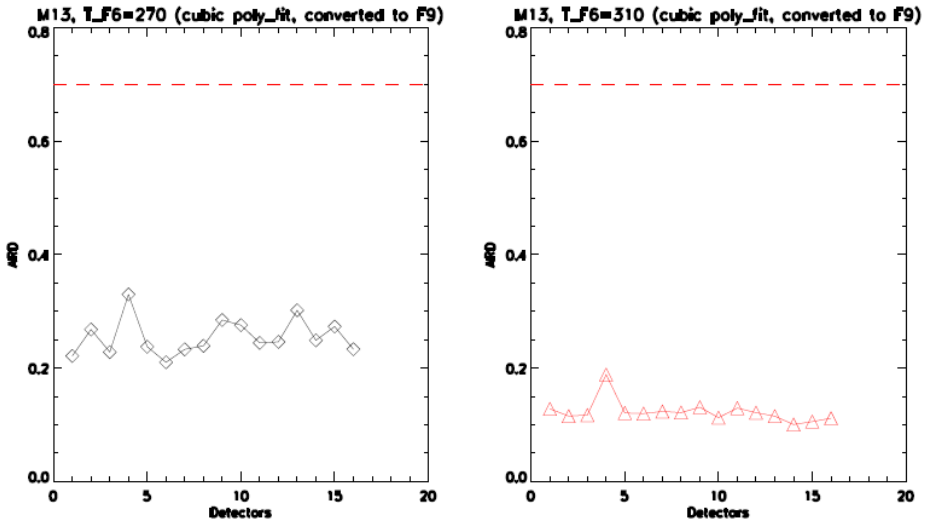

Figure 16: M14 ARD for HAM side A.

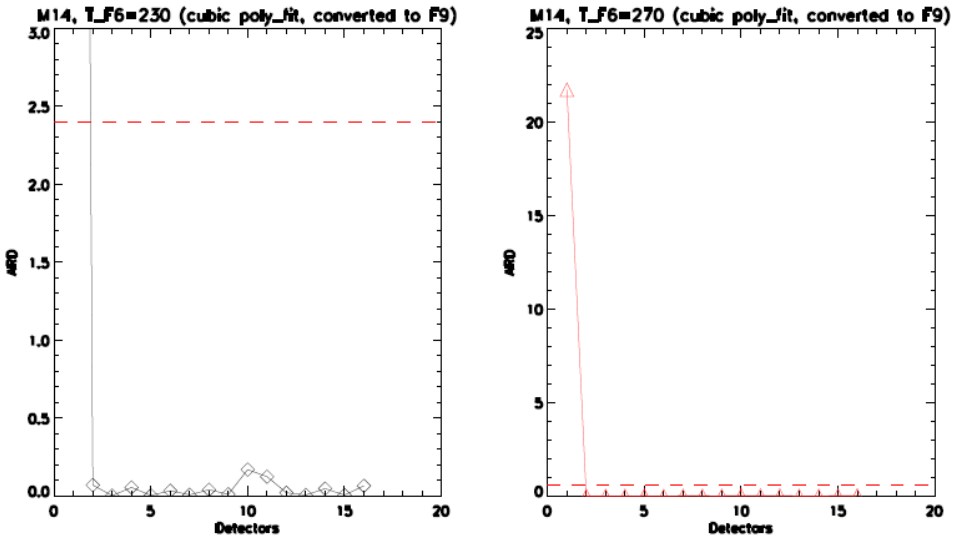


Figure 17: M15 ARD for HAM side A.

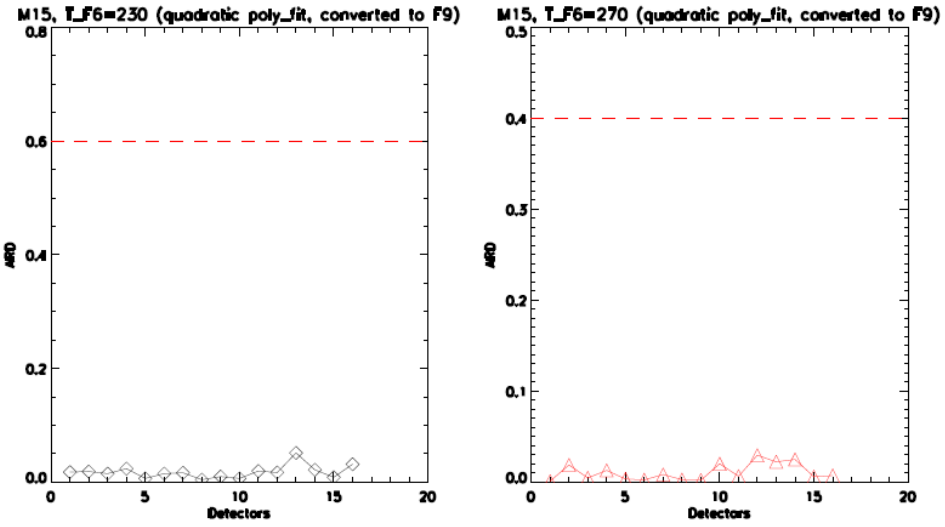

Figure 18: M16A ARD for HAM side A.

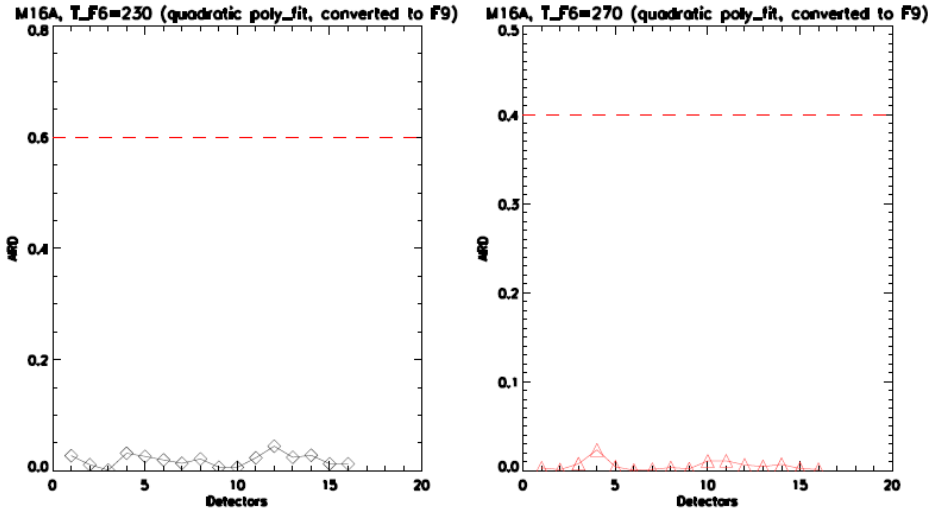


Figure 19: M16B ARD for HAM side A.

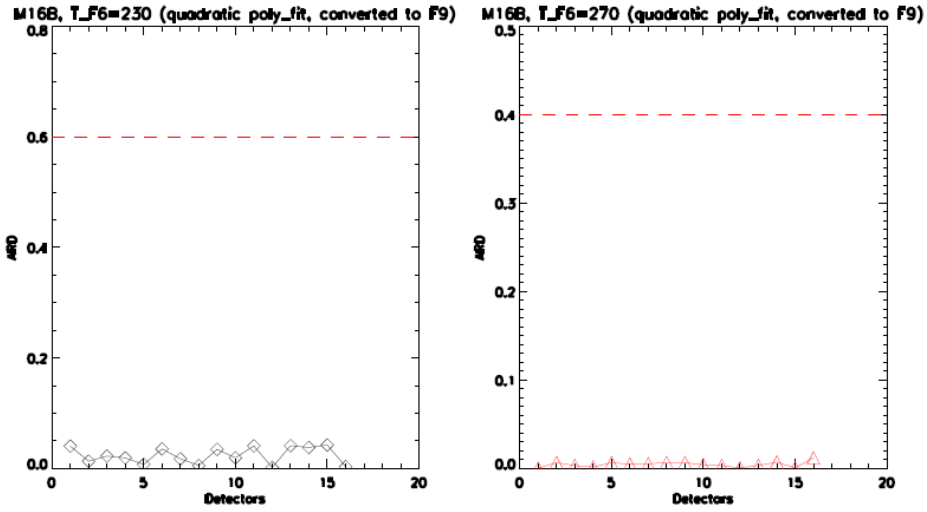
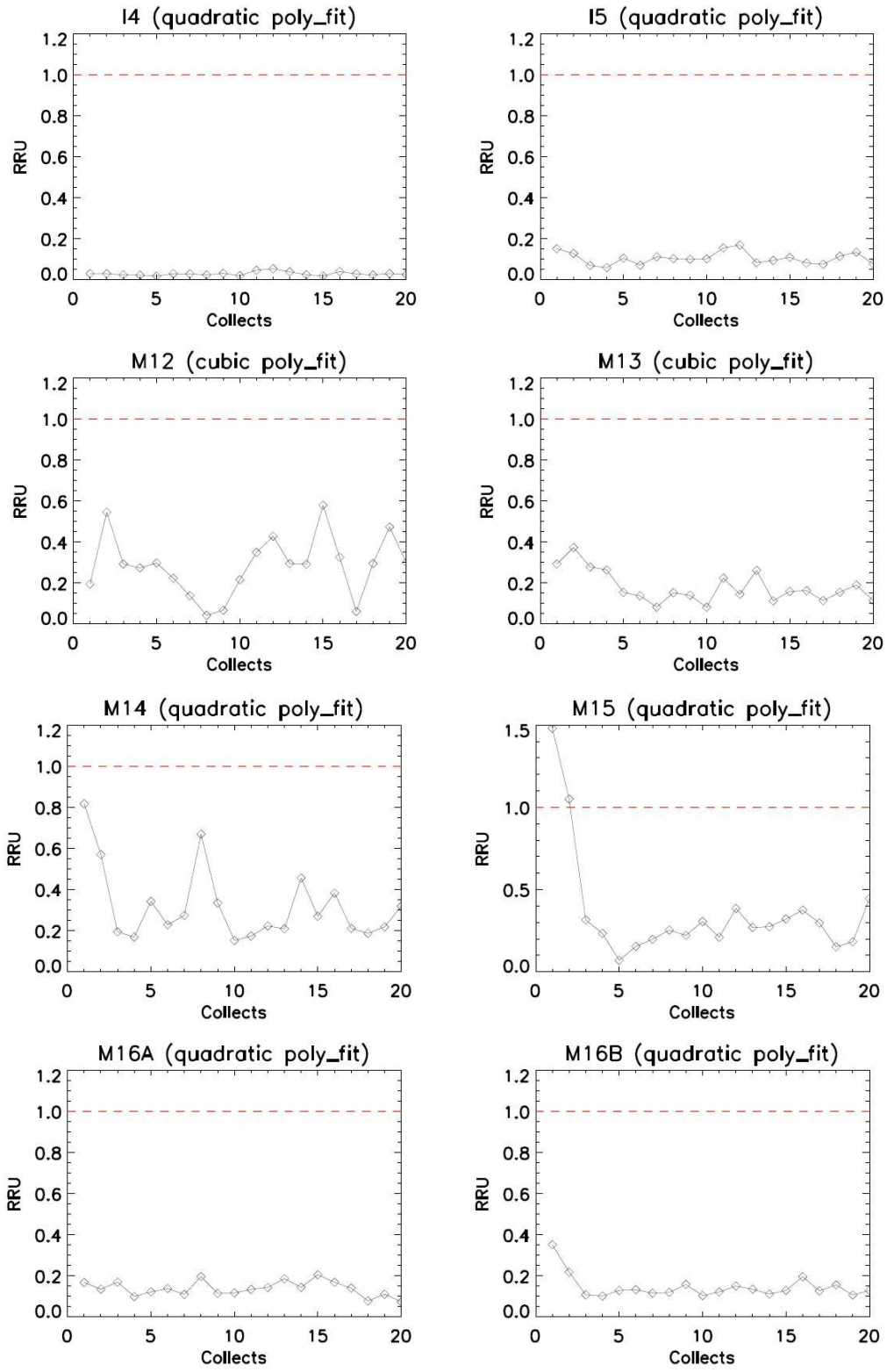
Figure 20: RRU for HAM side A (subsample 1 for I bands).